Phys Chem Minerals (1999) 26:275–296

ORIGINAL PAPER

J.F. Blackburn · E.K.H. Salje

Time evolution of twin domains in cordierite: a computer simulation study

Received: 11 March 1998 / Revised, accepted: 28 August 1998

Abstract The time and temperature evolution of twinning in cordierite is simulated using three computer models. The orientation of walls between twin domains in natural cordierite follows mainly the ferroelastic pattern which minimises the strain energy of the walls between twin-related domains. Such ferroelastic twinning is simulated in an elastic three-states Potts model in which each structural six-membered ring is represented by a three state pseudo-spin. The resulting twin pattern in a sample with 3169 structural rings shows sector trilling and fine scale ferroelastic wall patterns which coarsen with increasing annealing time. The poorly defined wall directions observed in cordierite were found to be related to twin walls which do not minimise the strain energy. Instead, these walls are located along the corners of pseudo-hexagonal rings and appear as the consequence of local rather than global interatomic interactions. Simulations using two-dimensional (38028 atoms) and three-dimensional (408 228 atoms) structural models show a predominance of these topological walls over the strain walls at early stages in the ordering process. The domain structure in the simulation is patchy rather than corresponding to repeated stripe structures found in other ferroelastic and co-elastic materials. In all models, a strong tendency for sector trilling is observed. In kinetic tweed patterns a novel 60º tweed is found at atomic length scales while the usual strain-mediated 90º tweed appears at mesoscopic length scales. An unusual surface tension effect in domain formation and 'writhing', fluid-like motion was found in the three-dimensional structural model. This motion, along with the existence of non strain-mediated walls may contribute to cordierite's poorly defined domain wall directions at the early stages of domain coarsening.

Key words Cordierite · Twin structure · Time evolution · Domain · Computer simulation

J.F. Blackburn · E.K.H. Salje (✉)
Department of Earth Sciences, University of Cambridge, Downing Street, Cambridge, CB2 3EQ, UK

1 Introduction

The fingerprint for the appearance of cordierite in petrological thin sections is its characteristic 'sector trilling' as shown in Fig. 1a for a sample of volcanic origin. Closer inspection of metamorphic and volcanic cordierite samples often reveals a surprisingly complex microstructure which includes jagged twin walls, needle domains of a rather broad, 'patchy' nature and rather wiggly twin walls which appear to bend and twist when viewed along the pseudo-hexagonal c-axis (Venkatesh 1954; Müller and Schreyer 1991). Such extreme bending of twin walls is uncommon in minerals because it requires large anisotropy energies and, in the case of thick walls, high bending energies (Salje and Ishibashi 1996; Salje et al. 1998). A typical example of the complex microstructure in cordierite is shown in Fig. 1b with jagged and curved walls, and needle domains clearly visible. The most surprising microstructural property of cordierite is its ability to form twin walls which are *not* compatible with the condition that two adjacent twins exert no stress on the wall. This condition defines elastically 'soft' planes. In all known ferroelastic materials, besides cordierite, twin walls are oriented along these soft planes.

In Fig. 1c an example of a cordierite sample is shown which displays the usual ferroelastic 'strain walls' and, in addition, twin walls which are rotated away from these elastic soft directions. These latter walls are not stress free and, for reasons to become clear later, will be referred to as 'topological walls'.

Figure 2 shows the early stages of tweed formation for synthetic cordierite analysed using TEM techniques. At these much smaller length scales we can see that the tweed pattern is extremely wiggly with very poorly defined wall directions compared with alkaline feldspars and YBCO (Putnis and Salje 1994). The domains also seem to form into small, isolated patches rather than the long, unbroken stripes observed in these other structures.

The question which is addressed relates to the origin of these unusual microstructures in cordierite. An intuitive

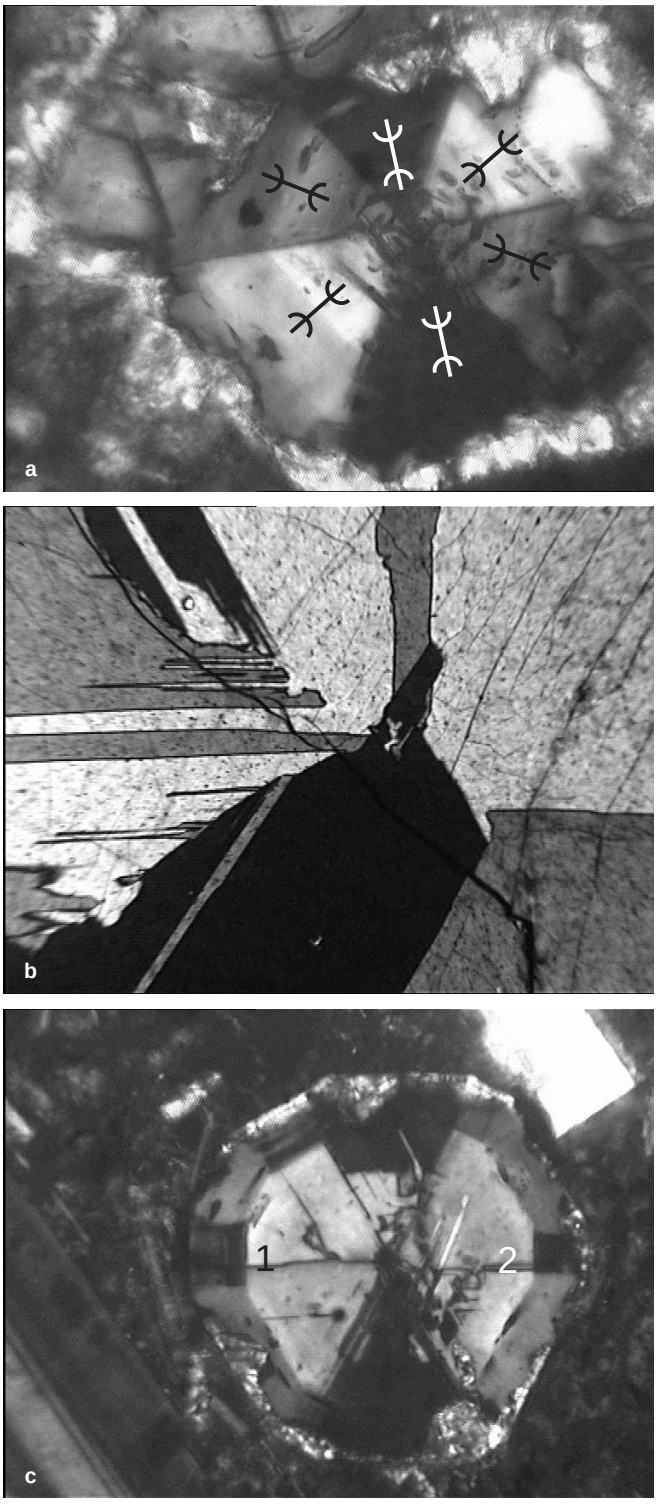

Fig. 1a–c Sector trilling in naturally occurring cordierite samples as observed under an optical microscope. **a** Sector trilling structure consisting only of strain-mediated domain walls. The optical axis directions are shown in each domain as calculated from birefringence analysis. These directions are discussed in Section 7. **b** Twinning and needle domain formation. **c** Sector trilling but with additional walls which are not strain mediated (marked *1* and *2*)

Fig. 2 Time evolution of synthetically grown cordierite. Starting from a hexagonal structure, tweed patterns form and then coarsen into twin domains. The scale bar shown is 0.2 μm long, (after Putnis et al. 1987)

answer might be expected from the outset. Let us start from the idea that the formation of twins in cordierite can be envisaged as the result of a transition between a hexagonal phase (P6/mcc) and an orthorhombic phase (Cccm). The hexagonal phase may exist as an equilibrium phase at temperatures above 1720 K (Müller and Schreyer 1991; Redfern et al. 1989; Schreyer 1986; Putnis et al.

1987; Salje 1987; Daniels et al. 1992) or as a kinetic precursor phase which nucleates within the stability field of the orthorhombic phase and subsequently undergoes a non-equilibrium ferroelastic phase transition. The topology of the crystal structure shows a (pseudo-) hexagonal atomic arrangement with twin formation along the hexagonal basal axes (Putnis and Salje 1994; Nord 1994). This process is in competition with the requirement that ferroelastic twin walls are perpendicular to each other, i.e. they break the hexagonal symmetry. As a result of the competition between the requirements of the atomic structure and the minimisation of the elastic strain energy one might expect the simultaneous appearance of two types of walls or a wall structure which represents some compromise between atomic and strain features.

The results of the study presented in this paper and the experimental evidence points clearly to the first solution of the two wall types with the additional observation that strain walls dominate over topological walls at late stages of the microstructural development.

Our analysis consists of computer simulations of three models with increasing complexity approaching a rather realistic cordierite structure. The process which leads to the formation of twins is the atomic ordering of Al and Si 'ordering atoms' within a complex network of oxygen tetrahedra.

Cordierite ($Mg_2Al_4Si_5O_{18}$) consists of two sublattices of atoms which behave in quite different ways. The Al and Si atoms are always located at the centres of oxygen tetrahedra but are able to move from one tetrahedron to another. The precise way in which they form into patterns dictates the degree of order in the system. Therefore these atoms are known as *ordering atoms*. The sublattice of Al and Si atoms forms a binary alloy.

In contrast, the rest of the lattice (consisting of Mg and O atoms) is known to be very rigid and these atoms can only move short distances from their mean positions: they never swap sites. The sublattice of Mg and O atoms is called the *host lattice*.

Al atoms are physically larger than Si atoms and so tetrahedra containing Al atoms 'swell up' and gain a greater volume than those with Si at their centres (Gibbs 1966). The four oxygen atoms at the vertices of these tetrahedra are therefore pushed outwards and in turn apply forces on neighbouring atoms. This knock-on effect causes a distortion in the host lattice which propagates throughout the crystal applying forces on other ordering atoms. Thus, the ordering atoms interact with each other indirectly via the host lattice which acts as an elastic background. This interaction is known to be long-ranging and anisotropic; its symmetry depends on that of the crystal structure (Bratkovsky et al. 1994a).

Because of this strain mediated interaction between ordering atoms, we would expect the types of domain walls allowed to be determined by strain effects which are independent on the precise atomic structure. This has indeed been the case in the computer simulations of other crystals studied in this way (Salje and Parlinkski 1991; Parlinski et al. 1993; Bratkovsky et al. 1994b, 1996; Tsatskis et al. 1994; Tsatskis and Salje 1996; Vul and Salje 1995). However here we will show that these strain mediated walls, while important are not the only allowed walls. In addition, there are topological walls formed due to local interactions between cordierites characteristic six-membered tetrahedral rings.

2 Crystal structure and domain walls

The structure of cordierite is shown in Fig. 3 (Gibbs 1966). It consists of two types of oxygen tetrahedra called T1 and T2. The T2 tetrahedra form layers of six-membered rings. In each unit cell, there are two layers of T2 rings with the rings in alternate layers rotated by 30º with respect to each other. The T1 tetrahedra form 'ladders' connecting these T2 layers. Al or Si atoms are present in each tetrahedron. There are also oxygen octahedra present with Mg atoms at their centres.

Domain formation occurs when each T2 ring contains 2 Al and 4 Si atoms and the Al atoms are aligned on opposite sides of the ring. Figure 4 shows one way in which this can happen. There are three ways of having this type of order and so there are three types of domain. Each ring has a domain type associated with it which we will denote by a number 1, 2 or 3. We will call this number the *ring spin* since it is analogous with spins found in ferromagnetic materials. In using this nomenclature we reduce the system to a three-state Potts model in three dimensions (e.g. Eichhorn and Binder 1996; Binder 1981).

There is a tendency to exclude two Al from being present in adjacent tetrahedra (Loewenstein's rule: Loewenstein, 1954) so that the 'spin' of a ring indicates the configuration of ordering atoms in that T2 ring and also in the *surrounding* ring of T1 tetrahedra (see Fig. 4). Thus the configuration of all ordering atoms in the crystal can be specified by stating the ring spin configuration.

In the computer simulation we will use the ring spin values shown in Fig. 5 to indicate the type of ordering in each T2 ring. Notice how we expect the Al opposite pairs in the two types of T2 rings to be aligned next to each other such that the Al-bearing T2 sites on each side of the ring are connected by T1 tetrahedra. The diagram also indicates how T2 tetrahedra with Al present swell up distorting the T2 ring into an elliptical shape.

The phase transition between hexagonal and orthorhombic cordierite leads to a symmetry reduction which is illustrated in Fig. 5. The strain formed as a result is caused by the opposite Al pair stretching the T2 ring out with a corresponding contraction in the perpendicular direction. This stretching is then transmitted to neighbouring rings causing a spontaneous strain of the form (Salje 1993):

$$\varepsilon = \begin{pmatrix} \varepsilon & 0 & 0 \\ 0 & -\varepsilon & 0 \\ 0 & 0 & 0 \end{pmatrix} \tag{1}$$

with respect to the strain's principle axes in each of the three domain types.

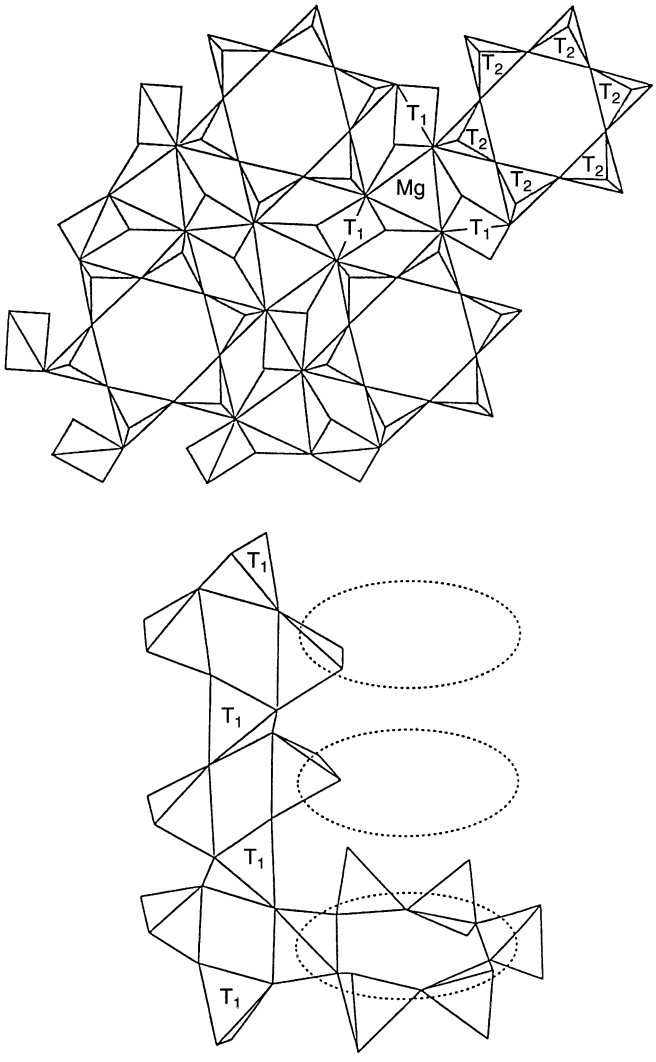

Fig. 3 The structure of cordierite in the a-b plane and along the c direction. T1 and T2 tetrahedra are shown (after Putnis 1992)

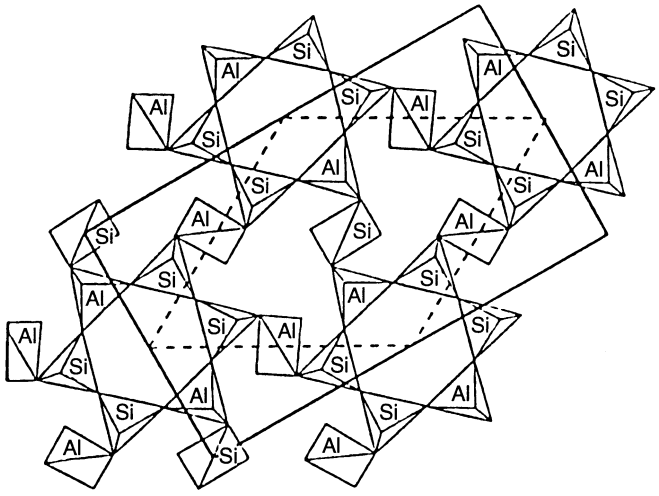

Fig. 4 Al/Si configuration in ordered cordierite. The *dashed lines* show the high temperature hexagonal unit cell and the *solid lines* show the orthorhombic unit cell which forms as a result of ordering below T_c, (after Putnis 1992)

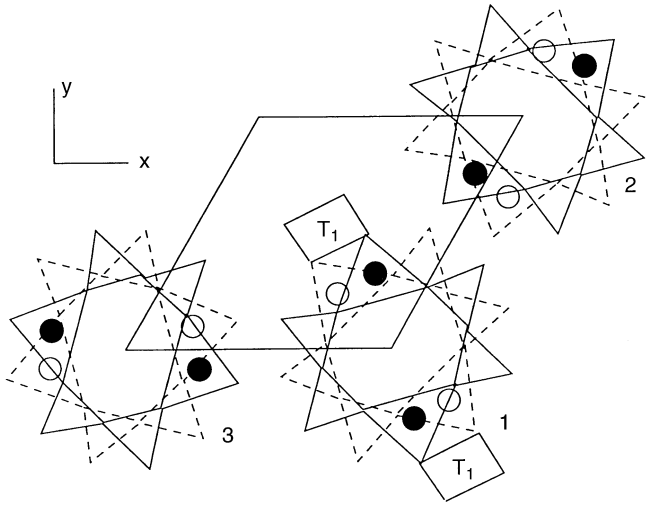

Fig. 5 The numbering system used to indicate Al opposite pair configurations in each ring. The axes shown are used throughout. The two types of T2 rings per unit cell are shown as *solid* and *dashed lines* and the Al positions are shown as *black* and *white circles* respectively. Other tetrahedra have Si atoms at their centres

When two domains come together the interface is called a *domain wall*. If the wall is strain mediated its orientation must be such that the strain a small distance away from the wall in both adjacent domains is the same (Sapriel 1975). Using this condition for a hexagonal/orthorhombic system, six walls of fixed direction perpendicular to the T2 planes are obtained:

Domain pair	Wall 1 angle	Wall 2 angle
1–2	0	+90
1–3	+60	−30
2–3	−60	+30

There are two mutually orthogonal walls between each pair of domains. The angles shown are with respect to the x-axis. These walls are shown schematically in the lower part of Fig. 6. As required by strain interactions, there are two mutually orthogonal walls for each domain pair. Structurally, the strain wall directions are located half way between the Al opposite pair orientations.

Three of the walls are formed by linking nearest neighbour T2 rings and we will call these *nn strain walls* whereas the other three link next-nearest neighbour T2 rings and will be referred to as *nnn strain walls*.

Also shown in Fig. 6 are six walls which are not strain related but do appear in the computer simulations. They are such that the Al pairs on one side of the wall are aligned along the wall direction (the domain on the other side being either of the other two types). We will call these walls *topological walls* since they relate to the local ring topology of cordierite rather than long ranging strain

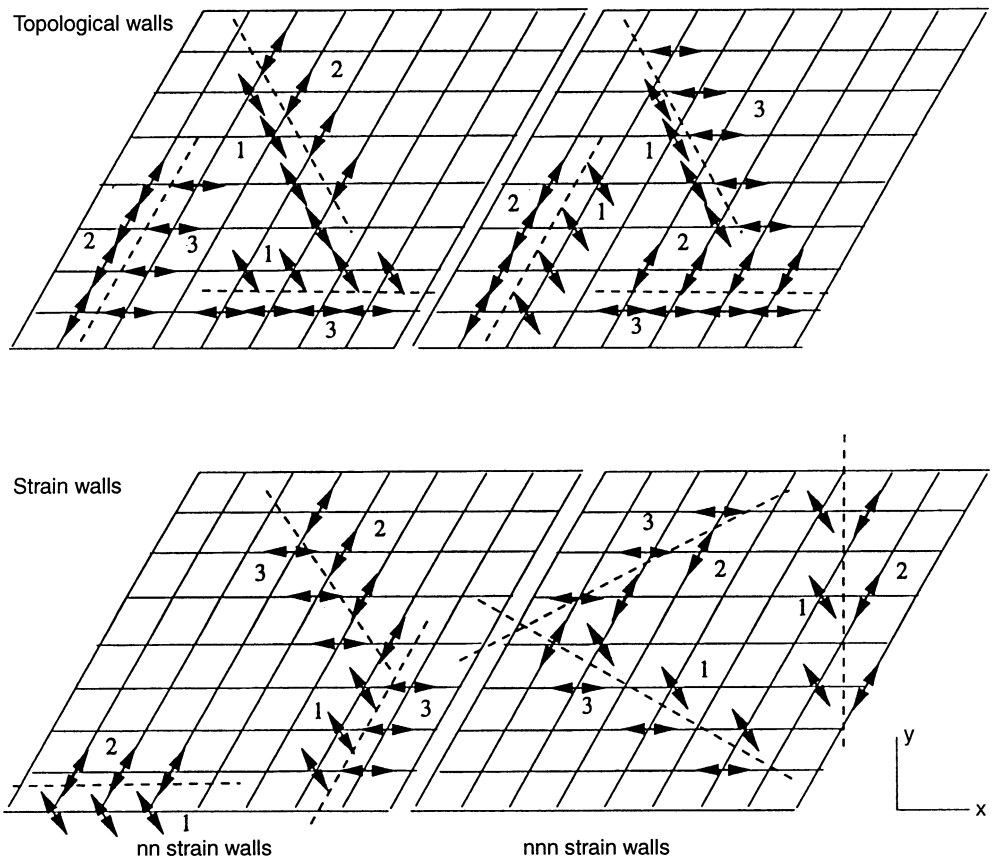

Fig. 6 The six strain walls and six topological walls observed in the simulation. A T2 ring is present at each line intersection in the diagram. The *double-headed arrows* indicate the direction of alignment of the opposite pairs of Al in the rings. In fact the actual Al positions are rotated by ±15° with respect to the arrow direction for the two non-equivalent T2 layers shown in Fig. 5. The *arrow* is drawn *half way* between these two orientations and also corresponds to the strain direction. The *dashed lines* indicate the wall directions

interactions which give rise to the strain walls. Thus cordierite displays 12 domain walls in total, 6 of which are ferroelastic in nature.

3 Computer models

The problem of cordierite ordering turns out to be considerably more complicated than that of any other material previously studied in this way. In order to understand the behaviour thoroughly and learn how different types of behaviour are governed by different structural elements we have carried out the simulation on three different levels of complexity, which are discussed individually in the following sections.

In all three models we use the following basic ideas. We assume that the host atoms interact with each other *harmonically*, i.e. that they are connected in a 'balls and springs' network. The exact strength and geometry of these springs is not known so we use such spring topology as to encapsulate our understanding of how cordierite behaves. Thus, the models are highly phenomenological: they are not based on exact interatomic potentials (which are irrelevant for large-scale microstructures) but on an elastic response which encapsulates the essential mechanisms for domain formation. It is technically impossible to explore the full parameter space of a structure of the complexity of cordierite, the best we can hope for is to get reasonable domain patterns which give us a 'feel' for the ordering behaviour.

The ordering atoms interact with nearby host atoms via constant 'Kanzaki' forces depending on the spin value of each T2 ring. We assume that the *direct* interaction between ordering atoms is comparatively weak and we ignore it. Thus, the Hamiltonian can be written as:

$$H = H_{\text{host}} + H_{\text{int}} \tag{2}$$

where H_{host} is the energy of the host atom-host atom interactions and H_{int} is the energy of the ordering atom-host atom interactions (Tsatskis and Salje 1996).

Because we are using simple spring bonds for the host lattice, we can write H_{host} as:

$$H_{\text{host}} = \sum_{\text{bonds}} \frac{1}{2} k_{\text{bond}} (\delta r)^2 \tag{3}$$

where δr is the stretching of a bond and k_{bond} is the spring constant. The sum is over all bonds in the host lattice. Using the formalism of the dynamical matrix we can rewrite this as

$$H_{\text{host}} = \frac{1}{2} u^T A u = \frac{1}{2} \sum_{nm} \sum_{ij} u_n^i A_{nm}^{ij} u_m^j \tag{4}$$

with the first expression written in matrix format (the matrices must be appropriately partitioned so as to include

the indices n, m, i, j). u_n^i is the ith displacement component of atom n and A_{nm}^{ij} represents the spring interaction between the i and jth displacement components of atoms n and m.

The force on each host atom, n, denoted f_n^i (with i corresponding to the Cartesian component) is given by:

$$f_n^i = \sum_{l\alpha} F_{nl}^{i\alpha} p_l^{\alpha} \tag{5}$$

where p_l^{α}, the occupation number indicates the presence or absence of an ordering atom of type α at site l such that $p = 1$ if the atom is present and $p = 0$ if the atom is absent. In cordierite, for example, we could take $p_l^1 = 1$ to represent the presence of an Al at site l and $p_l^0 = 1$ to indicate a Si. The matrix element $F_{nl}^{i\alpha}$ represents the ith component of force applied to atom n when an ordering atom of type α is present at site l. The matrix F therefore gives the set of Kanzaki forces.

Since the Kanzaki forces are constant, we can now write the total Hamiltonian as:

$$\begin{aligned} H &= \frac{1}{2} u^T A u - u^T F p \\ &= \frac{1}{2} \sum_{nm} \sum_{ij} u_n^i A_{nm}^{ij} u_m^j - \sum_{nl} \sum_{i} \sum_{\alpha} u_n^i F_{nl}^{i\alpha} p_l^{\alpha}. \end{aligned} \tag{6}$$

The evolution of the ordering atom configuration is modelled using the standard Metropolis algorithm of Monte Carlo analysis, interchanges of ordering atoms are attempted and the attempts accepted with probability

$$p(\Delta E) = \frac{\exp(-\Delta E / k_B T)}{1 + \exp(-\Delta E / k_B T)}. \tag{7}$$

Thus the system performs a 'random walk' from its initial configuration. Making use of the ergodic nature of the system, we can take the evolution of the system as it 'walks' to correspond to its *time evolution*. The number of Monte Carlo steps, t_{MC} is related to the real time elapsed, t by:

$$t = t_{MC} \exp(E_a / k_B T) \tag{8}$$

where E_a is some characteristic activation energy of the Monte Carlo interchange. Thus a sequence of spin configuration snapshots represents the time evolution of the system.

In the computer simulation we are only interested in the motion of the ordering atoms since these dictate domain formation. The host atoms are necessary only as an elastic medium with the required stiffness and geometry to cause the correct interactions between ordering atoms. In order to express this interaction most clearly, we allow the host lattice to relax to its minimum energy configuration between interchanges of ordering atoms. This also allows us to eliminate the host atom displacements from Eq. 6 and hence reduce the model to a Potts model.

Minimising Eq. 6 with respect to atomic displacements gives:

$$\frac{\partial H}{\partial u_n^i} = (A u - F p)_n^i = 0 \tag{9}$$

which leads to the matrix of relaxed displacements,

$$(u_0)_n^i = \left(A^{-1} F p\right)_n^i. \tag{10}$$

Substituting this back into Eq. 6 yields:

$$H_0 = \frac{1}{2} p^T V p \tag{11}$$

with,

$$V_{lk}^{\alpha\beta} = -\left(F^T A^{-1} F\right)_{lk}^{\alpha\beta}. \tag{12}$$

This is the Hamiltonian used in the simulation. It is formally the same as that of a Potts model with a highly complex interaction term V. While in nearest-neighbour Potts models most elements of V are zero *none* of the elements are zero in our simulation. In fact, the interaction can be shown to decrease as R^3 where R is the distance between ordering atoms so it is indeed long ranging as we expect. The anisotropy of the interaction of the system can also be derived from an analysis of Eq. 11 (Bratkovsky et al. 1994a).

One way to calculate the energy differences required for the Metropolis algorithm would be to calculate the tensor V from the springs and Kanzaki forces of the system. However the number of atoms considered in these simulations is very large (of order 10^5) and the size of the dynamical matrix A is $(dN)^2$ where d is the dimensionality and N the number of host atoms. It is impractical to attempt to invert such a large matrix and so Newtonian molecular dynamics with damping is used to move the host atoms to their lowest energy positions and minimise the energy in Eq. 6.

The most straightforward way to proceed would be to calculate the energy for a relaxed system (using molecular dynamics), interchange ordering atoms, recalculate the energy and subtract to get the energy change for Eq. 7. However, the relaxation process for such a large number of atoms is very computationally intensive and doing two relaxations per interchange requires too long a computational time.

Instead of calculating ΔE directly, we calculate the quantity

$$\Delta \tilde{E} = -u_0 F \Delta p \tag{13}$$

where u_0 is the set of relaxed host atom displacements and Δp is the difference in the ordering atom configuration due to one Monte Carlo interchange. This quantity turns out to be related to ΔE by

$$\Delta E = \Delta \tilde{E} + \delta \tag{14}$$

where δ is the *energy correction*. It is a constant which depends only on the structure of the model and can be cal-

culated before running the simulation. This calculation will be discussed in more detail in the later sections with respect to each model in turn.

The computer algorithm then operates as follows: the host lattice is relaxed, *all* Monte Carlo interchanges in the lattice are attempted at once and the process is repeated. Thus all the ring spins can be changed for a single host lattice relaxation.

We use free boundary conditions throughout rather than the more usual periodic boundaries because the latter tend to produce a spurious periodicity in the spin configurations generated by the simulation. Periodic boundaries also prevent the formation of large-wavelength stretching modes in the host lattice (such as an overall volume expansion) which we expect to observe.

All the simulations are carried out from an initial random ring spin configuration and so correspond to a quench from infinite temperature or the time evolution from a hexagonal precursor phase.

The computer programs were run on the Hitachi S-3600 vector computer, part of the Cambridge University High Performance Computing Facility.

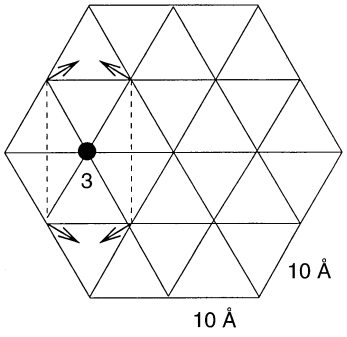

Fig. 7 The three states strain Potts model. Each intersection in the diagram represents an atom *and* a 'ring spin'. The *lines* shown are the host lattice springs. The forces applied due to a spin of type three being present at the *point* marked by the *circle* are shown as *arrows*. Equivalent forces are applied by ring spin types 1 and 2 but rotated by ±60°

4 A 3-states strain-mediated Potts model

4.1 Methodology

The essential features of the hexagonal to orthorhombic phase transition and the elastic nature of the host lattice interactions are captured in a simple, 'toy' model with only one atom per unit cell. As the long ranging elastic interactions guarantee that the phase transition follows mean field behaviour, the dimensionality of the lattice becomes irrelevant ($d \geq 2$). The simulation is done in the least allowable dimension, namely $d = 2$.

Figure 7 shows a schematic diagram of the system. There is one atom (representing the entire T2 ring) and one ring spin present at each intersection in the diagram and the lines represent springs connecting nearest neighbour host atoms. The forces are applied such that the host lattice stretches to produce the spontaneous strain expected when each type of ring spin is present at the corresponding site.

We do not have anything corresponding directly to Al or Si ordering atoms in this simulation, instead the ring spins apply forces directly. The occupation numbers in Eq. 5 now correspond to the configuration of ring spins such that $p_l^\alpha = 1$ implies that a ring spin of type α (1, 2 or 3) is present at site l.

Because this system is truly a three state model, it turns out that the energy correction can only be expressed in terms of A^{-1} which as we have noted is hard to calculate. However, experience with similar systems (with only one atom per unit cell) has shown that the energy correction is rather small compared to typical values of $\Delta\tilde{E}$ encountered during the simulation. For the simple model, therefore we ignore this correction and use $\Delta\tilde{E}$ to represent the energy changes.

A 2D hexagonal sample was used with 32 atoms on a side of the hexagon giving 3169 atoms and ring spins in total. The overall hexagonal shape of the total sample turns out to be necessary in order to produce the correct symmetry above T_c.

4.2 Results and discussion

Figure 8 shows the 'time' evolution of the ring spins in the simple model at $T = 0.2\,T_c$ (T_c was calculated by plotting the average magnetisation of the sample as a function of temperature). At this low temperature, the simulation shows very rapid domain formation and coarsening. The walls which form are the strain walls described in Fig. 6, with no sign of any topological walls. For example at t=60 Monte Carlo steps per ring (MCSPR) we see all six strain walls in one plot. The 90° angles between like strain walls are clearly visible in this snapshot for example the 1–2 vertical wall going upwards from coordinate (−30,0) and approaching its horizontal counterpart at around y=210. On the right hand side of the same figure, we can also see two 90° angles between three 1–3 walls.

In other similar simulations such as the square lattice (Bratkovsky et al. 1994b, Salje and Parlinski 1991), there is a strong tendency to form sets of parallel walls with alternating domain types in between. This periodicity is not observed here. Instead the domains tend to form into isolated 'islands'. The picture is fundamentally patchy with the size of the patches increasing with MC steps.

Coarsening continues rapidly with the larger domains growing indefinitely at the expense of the smaller ones. At t=300 MCSPR, we see only three large domains covering the whole sample.

The contrast between the periodic domains formed in other structures and the patchy cordierite domains shown here seems to correspond to experimental evidence from TEM pictures (Putnis and Salje 1994). The most striking effect of this is the formation of 'trilling' patterns in cordierite where domain growth increases into the macroscopic scale with sections of the material consisting of 3–6 domains each several millimetres across. Other materials such as alkali feldspar do not exhibit this effect and continue to show periodic twin domains even after very long annealing times.

Figure 9 shows the early formation of domains at the same temperature. After only a few MCSPR, the domains formed are very small and intersect each other in a complex network. This picture corresponds to the *kinetic*

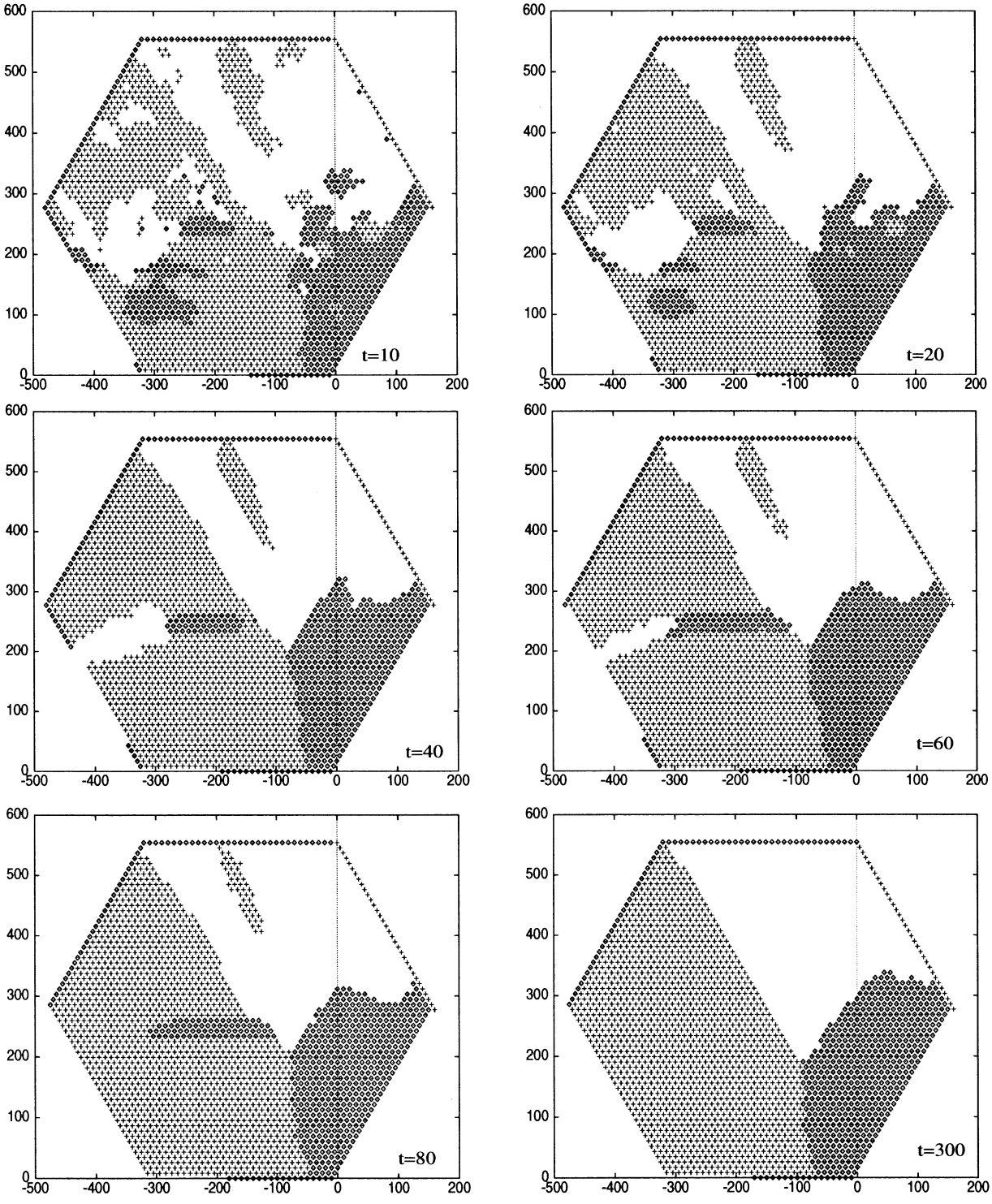

Fig. 8 Time evolution of the strain model from a random configuration at $T = 0.2T_c$. The *circles* are type 1 ring spins, the *crosses* type 2 and type 3 are not shown (*white*). The number of MC steps per ring (MCSPR) is indicated for each snapshot. The x-y coordinate axes shown are used throughout and correspond to those of previous figures

tweed structure, i.e. the tweed which is formed in the early stages of annealing as the system is driven towards coarsening well below T_c.

The walls appearing in these diagrams seem to be the nn strain walls rather than the nnn walls, which do not appear clearly until the later stages of domain evolution such as in Fig. 8. The nn walls appear to be favoured on the small length scales corresponding to the small domains formed at this stage.

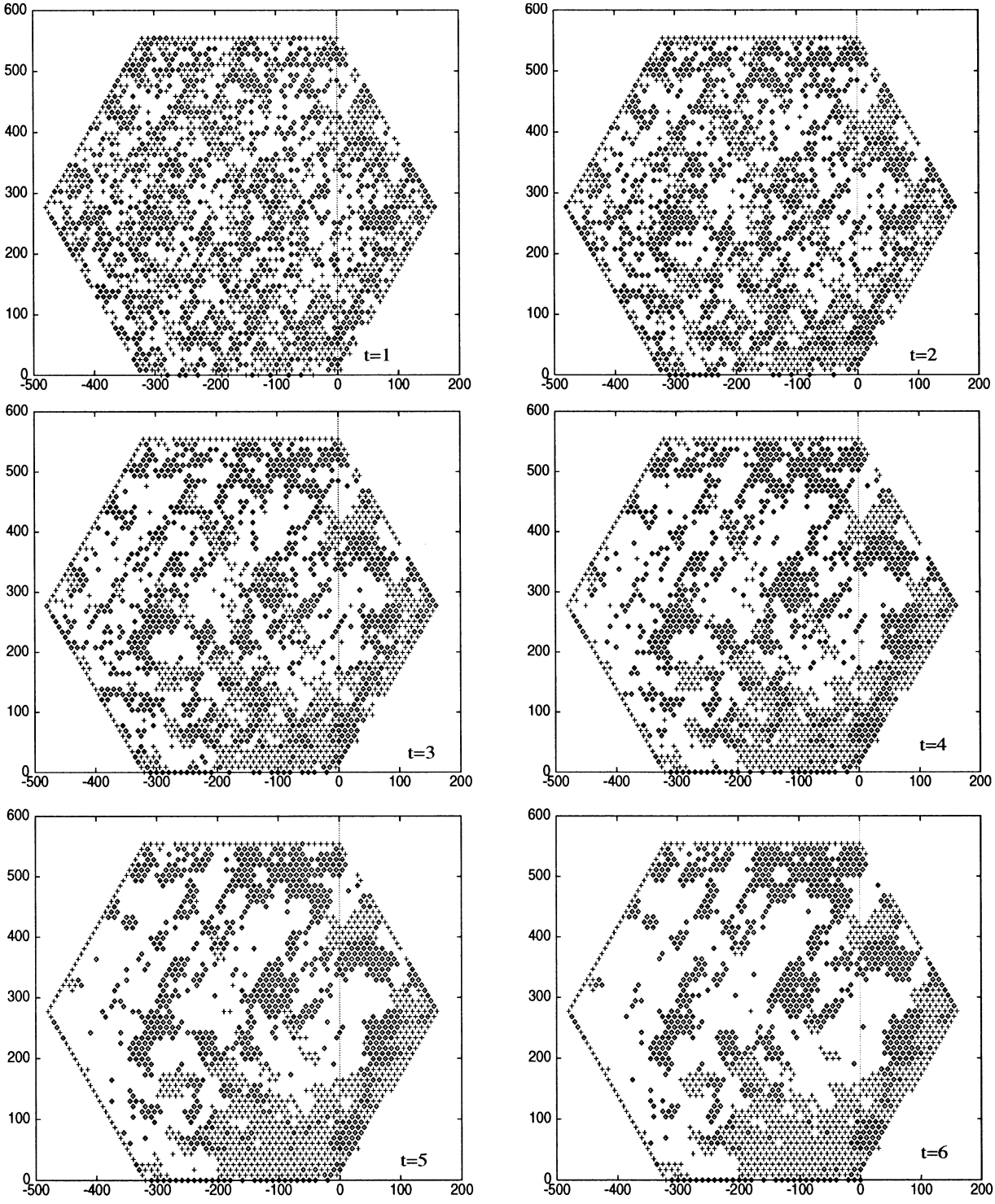

Fig. 9 Early evolution in strain model (°=type 1; +=type 2; blank= type 3)

To analyse this tweed pattern more rigorously, the *structure factor* was calculated. The structure factor is defined as the Fourier transform of the ensemble average of the spin correlation of the system (Tsatskis et al. 1994). Here, we use occupation numbers similar to those of Eq. 5 to specify the ring spin configuration such that $p_l^\alpha = 1$ if a ring spin is of type α at site l and 0 otherwise. A separate structure factor is then calculated for each ring spin type:

$$S^\alpha(\mathbf{k}) = 1 \Big/ \sqrt{N} \sum_{l-l'} \langle p_l^\alpha p_{l'}^\alpha \rangle \exp(\mathbf{k}.(\mathbf{r}_l - \mathbf{r}_{l'})) \qquad (15)$$

where $\mathbf{r}_l$ is the position of a ring spin and N is the total number of rings. We can express this quantity in the following form:

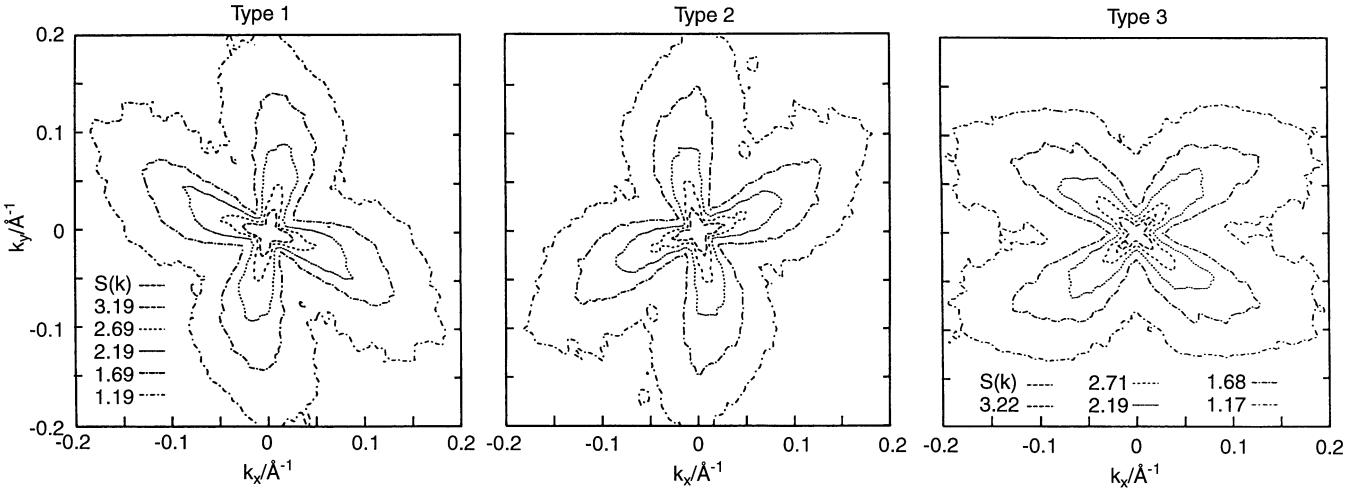

Fig. 10 Structure factor plots for the kinetic tweed structure of the strain model taken with respect to the three spin types shown

$$S^{\alpha}(\mathbf{k}) = \left\langle |p^{\alpha}(\mathbf{k})|^2 \right\rangle \tag{16}$$

which is easier to calculate on the computer.

Figure 10 shows the three structure factors. In our simulation, the Brillouin zone is a hexagon of diameter 0.8 Å^{-1} so the plots show about half of k-space centered at $\mathbf{k} = \mathbf{0}$.

Looking at $\alpha = 1$ first, we see there are two types of soft direction at different length scales. At short distances, further from $\mathbf{k} = \mathbf{0}$ we see two soft directions which appear to be perpendicular to the 1–2 and 1–3 nn strain walls in Fig. 6. Comparing this with the $\alpha = 2, 3$ plots we again see soft directions perpendicular to the *nn* strain walls involving types 2 and 3 again at short length scales far from $\mathbf{k} = \mathbf{0}$. This seems to indicate that the fine tweed (at short length scales) consists only of the *nn* strain walls which is consistent with the appearance of Fig. 9.

As we move towards the origin and longer length scales we see that the soft directions rotate until an orthogonal cross appears near the centre in each plot. This rotation is such as to include the soft directions perpendicular to the nnn strain walls.

For example, in the $\alpha = 1$ plot, we see the effect of the 1–2 and 1–3 *nnn* strain walls causing rotation away from +90° and −30° towards +60° and 0°. The near vertical direction at this length scale includes the 1–2 *nn* and the 1–3 *nnn* directions. The other direction refers to the 1–2 *nnn* and 1–3 *nn* directions. Thus the central 90° cross consists of two pairs of mutually orthogonal directions corresponding to all four walls associated with type 1 rings. The orthogonal crosses in the other two pictures similarly represent the four soft directions associated with ring spin types 2 and 3. Thus we observe two types of tweed formation: 60° tweed at short (atomic) length scales and more usual 90° tweed at longer length scales.

Figure 11 shows domain formation at $T = 0.6\,T_c$. At this higher temperature, we see that thermal effects introduce random fluctuations causing the domain walls to become much less distinct than before. There are also random patches of ring spins appearing within the domains themselves. Increasing the temperature further causes these fluctuations to increase until the spin distribution becomes approximately random.

Strain walls appear in this simulation as before. For example, we can see the 90° angle between the two 2–3 strain walls in the *t*=300 MCSPR snapshot. However, other walls (such as the 1–3 walls at the top and bottom of the same picture) are much less well defined: it appears that the soft directions are starting to become indistinct at this higher temperature.

Figure 12 shows the domain formation near T_c. Six different runs are shown from different, initial random configurations after 20 MCSPR each. The local domain wall directions have almost entirely broken down at this point. Instead, a small number of very large though poorly defined domains appear. Although we are at a very much smaller length scales, these pictures seem to correspond rather clearly to the trilling observed experimentally (Fig. 1). In particular, runs 3, 5 and 6 show 'sector trilling' with the hexagonal sample divided into six triangles and opposite triangles containing domains of the same type. This pattern is very commonly observed at these temperatures and seems to correspond to domains percolating across the sample and interacting with the sample edges.

As the temperature is very high in this case there are strong fluctuations with 20% of ring spins being changed at each step compared with Fig. 8 where the number of spin changes approaches zero by *t*=300. However, the overall shapes of the domains although poorly defined do remain fairly constant. The domains co-exist in a dynamical equilibrium compared to the static equilibrium established in Fig. 8.

The wall directions at these temperatures are very unclear and a structure factor plot such as Fig. 10 is dominated by the large trilling domains corresponding to peaks appearing near $\mathbf{k} = \mathbf{0}$. So it appears that the tendency to form domains survives at much higher temperatures than the tendency to form repeating twin structures with clear

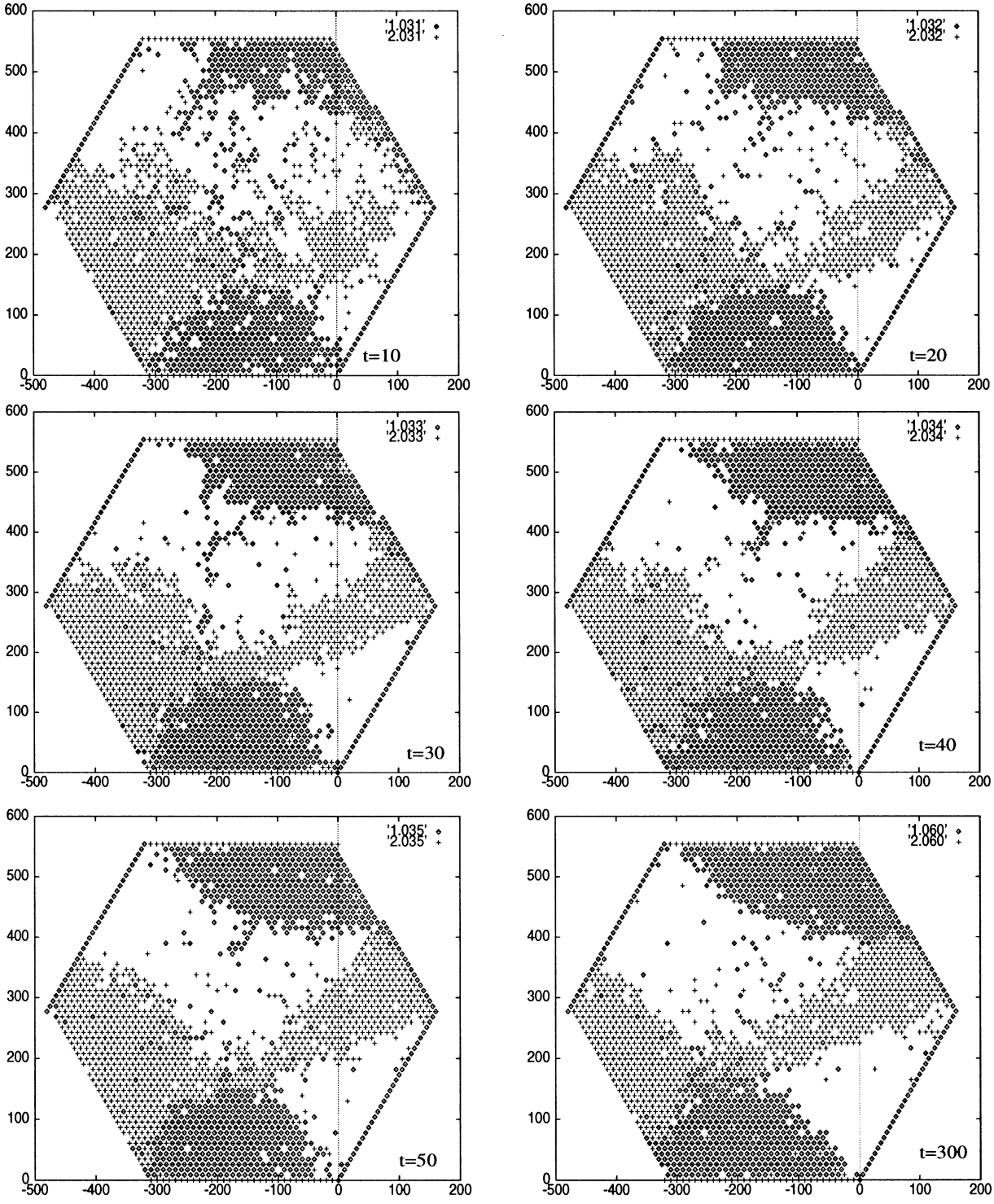

Fig. 11 Domain formation at $T = 0.6T_c$ (°=type 1; +=type 2; blank=type 3)

directionality. This is again suggestive of cordierite's patchy, large-scale domain formation, and its rather weak tendency to form walls perpendicular to elastically soft directions.

5 A two dimensional structural model

5.1 Methodology

In this model, we set up a direct analogue of the cordierite structure but in 2D. As strain interactions are rather well reproduced in two dimensions (Parlinski et al. 1993) it is now only the local interactions which may be oversimplified in this representation.

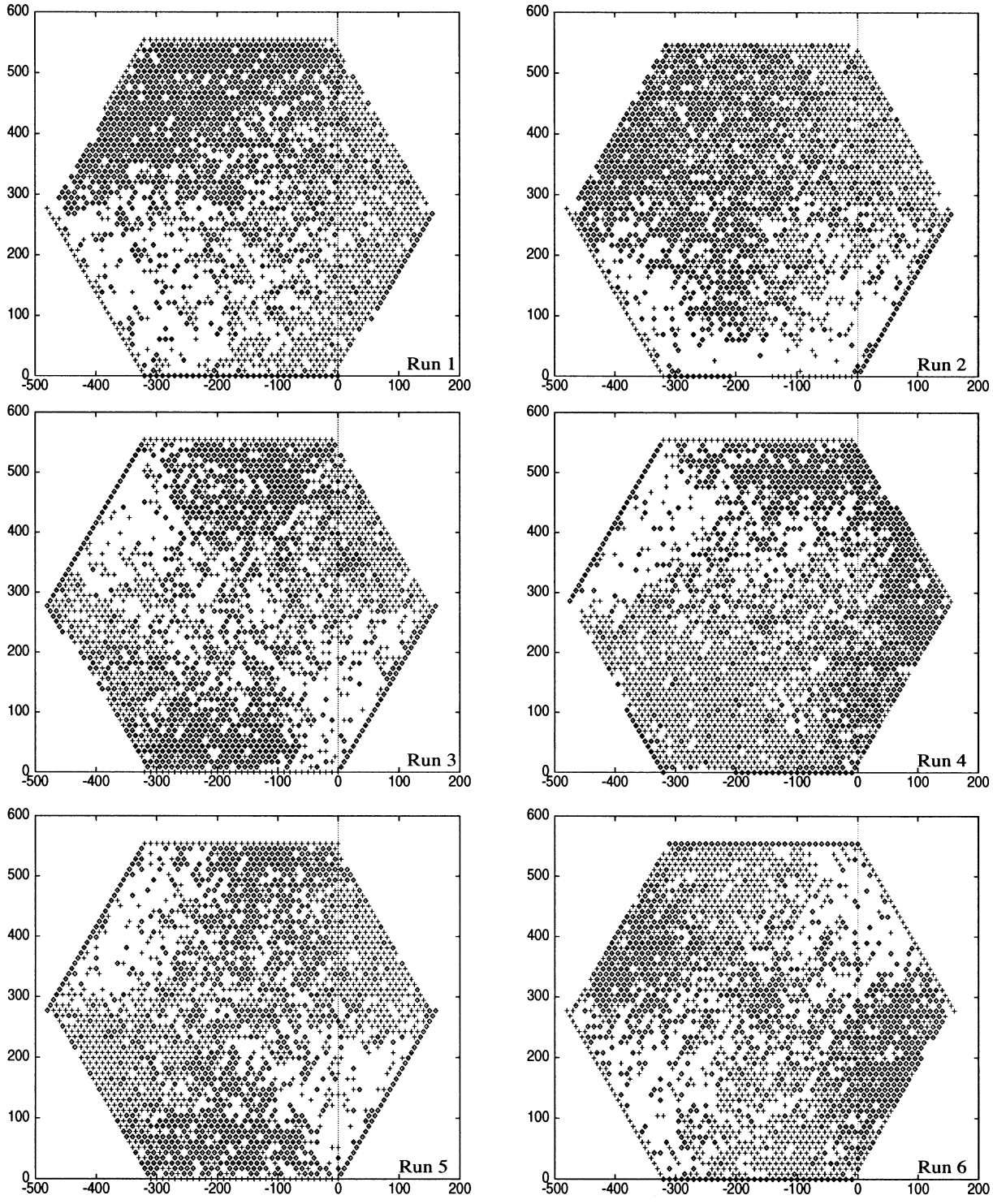

Fig. 12 Six different runs each at $T = T_c$ after 20 MCSPR each

Returning to the full 3D structure defined in Fig. 5, we imagine rotating the two types of T2 rings together and at the same time compressing them into a 2D sheet as shown in Fig. 13. The T2 tetrahedra become triangles and the T1s become single lines connecting T2 tetrahedra in neighbouring rings. We now wish to include three pieces of physics into the system: the swelling of the 'tetrahedra' (now triangles) in the presence of Al, the consequent distortion of the T2 rings into ellipses and the interaction between distorted rings which causes the strain and hence the ordering.

The tetrahedra encountered in all these structures are known to be rather rigid and so the oxygen atoms at the vertices of the T2 triangles are connected together using relatively strong springs (k=100 rel. units). The line which is all that now remains of the T1 ladders is also expressed as a spring (k=100 rel. units). In this form, the T2 ring would be very floppy and we expect it to behave as a fairly well-defined rigid unit so additional springs (k=50 rel. units) are added inside and outside the ring to stabilise its structure.

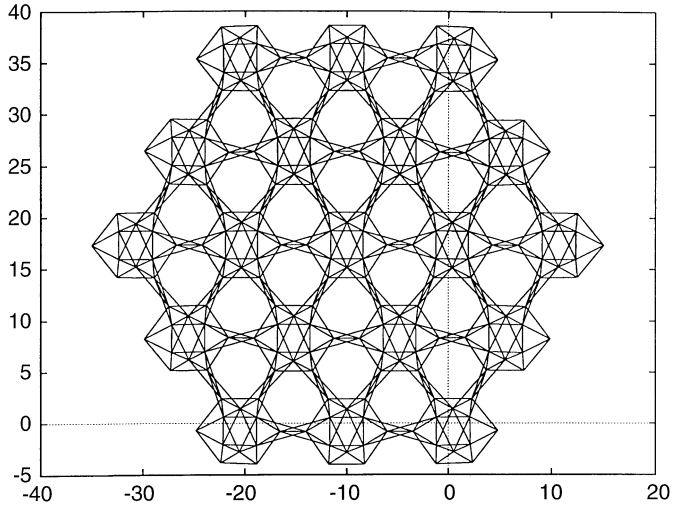

Fig. 13 The 2D structural model. The *lines* represent springs connecting oxygen atoms. This sample consists of a single type 3 domain and we can see that the T2 triangles containing Al are swollen with a consequent distortion of the rings causing the crystal to lose symmetry and become orthorhombic. The model used in the simulations has 32 rings on a side of the hexagonal sample rather than three shown here

Finally, some additional springs are connected between rings to increase the ring-ring interaction (k=200 rel. units). In particular, these last set of springs encourage Al atoms to align next to each other in neighbouring T2 rings so producing ferroelastic ordering with adjacent ring spins being of the same type. The resulting system is shown in Fig. 13.

This simulation incorporates all the physical mechanisms we believe are important in cordierite ordering with the simplest possible geometry. This simplified model not only saves computer time but also exhibits the ordering behaviour most clearly without the 'distraction' of higher order 3D structures.

Returning to Eq. 5 we use the occupation numbers p to represent the presence of either Al or Si in the centres of the T2 triangles. The forces are such that when an Al is present in a triangle its oxygen atoms are pushed outwards by Kanzaki forces drawn outwards from the triangle's centre of mass. *No* forces are applied when Si atoms are present.

The only ordering atom changes allowed during the system are such that each ring configuration changes from one opposite-Al configuration in Fig. 5 to another. Thus each Monte Carlo step involves changing two Si into Al and two Al into Si i.e. *rotating* the Al pair from one ring spin configuration to another. Previous attempts at using Kawasaki dynamics to interchange nearest neighbour pairs of ordering atoms failed to produce the ordering patterns described in Fig. 5, so it appears that this restriction is computationally necessary. The tendency of ordering atoms to form into patterns other than those shown in Figs. 4 and 5 was identified by Thayaparam et al. (1996) who considered such configurations to represent an intermediate phase between disorder and the order observed experimentally in Fig. 1 and described in Fig. 5. Since we only wish to analyse this latter type of ordering, we restrict the ordering atom configurations as described.

Because the occupation numbers now refer to the two ordering atoms rather than the three ring spins, it is possible to calculate the self-energy correction from a sequence of lattice relaxations. If we consider a particular ring at the centre of a hexagonal sample and imagine that the rest of the lattice apart from this ring contains no ordering atoms (and so no Kanzaki forces are applied to the atoms in other rings), then E_0 is the relaxed energy of a single Al placed at any of the six sites in this ring (all six sites are symmetrically identical). E_1 is the energy of two Als placed next to each other in the ring; E_2 is the energy of two Als placed next *but one* to each other and E_{opp} is the energy of two Al placed opposite each other (just like in an ordered system). The energy correction can then be shown to be given by

$$\delta = 8E_0 + 2E_{opp} - 2E_1 - 2E_2 \tag{17}$$

and this value was calculated before running the simulations. The parameter, δ was used to calculate ΔE for each ring rotation as described in Eqs. 13 and 14.

A 2D hexagonal sample was used with 32 rings on each side of the hexagon and 38028 atoms in total.

5.2 Results and discussion

Figure 14 shows the ring spin evolution below T_c for this 2D model. From the start (at t=10 MCSPR) we see the formation of *topological walls*: type 1 spin domains tend to have +60° walls, type 2 −60° and type 3 0°. In each case, the walls are parallel to the opposite Al pair direction corresponding to topological walls. This is just as shown in Fig. 6.

As the simulation proceeds and the domains begin to coarsen, we see the emergence of nnn strain walls such as the vertical 1–2 wall in the t=2000 plot. However, topological walls still seem to make an important contribution to the domain patterns even for these larger domains. For example, in the t=150 snapshot, we see a +60° 1–2 topological wall on the right of the diagram and a −60° 1–2 wall on the left. The t=2000 snapshot shows a 0° 2–3 topological wall.

The *nn* strain walls seem to be entirely absent from these pictures and many other simulations (with the same structure but different initial random configurations) seem to confirm this. It seems that the topological walls suppress the formation of *nn* walls because they are along the same directions. The *nnn* strain walls are along different directions from the topological walls and so continue to appear.

The coarsening process here is rather similar to that of Fig. 8: patchy domains form with little evidence of striped, repeating patterns. The large domains grow at the expense of the smaller ones until the sample consists of three large domains: one of each type.

The formation of these topological walls is not observed in the simple model and so we conclude that these walls are caused by the ring structure associated with each unit cell. The mechanism of swelling tetrahedra and stretching ellipses gives rise to an additional thermodynamically favoured pathway: the formation of walls along the Al pair directions, i.e. topological walls.

Whereas the strain interaction is very long ranging and insensitive to the precise topology of the unit cell, these walls seem to be caused by the direct 'rubbing' together of nearby elliptical rings. We conclude that the topological walls are a direct result of the atomic *ring structure* of cordierite.

Figure 15 shows the atom positions for a topological wall, an *nn* strain wall and an *nnn* strain wall as formed in this simulation. The Al bearing T2 triangles are swollen up whereas the Si bearing triangles are somewhat crushed. The rings next to the walls show some further distortion and there appears to be a tendency for oxygen

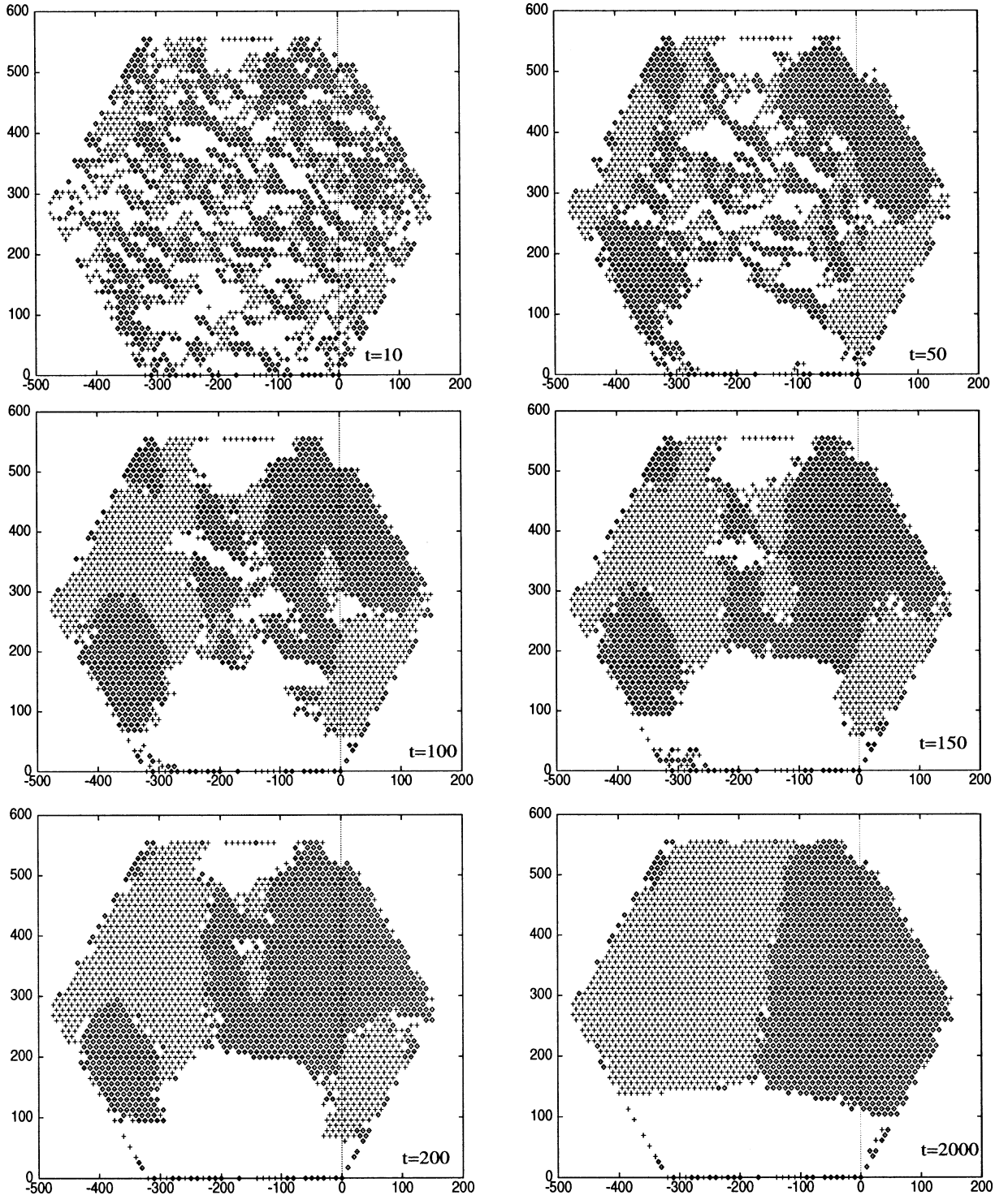

Fig. 14 Time evolution of 2D structural model at $T = 0.01\,T_c$ (°=type 1; +=type 2; blank=type 3)

atoms near the wall to move towards it distorting the triangles to which they belong.

Figure 16 shows the evolution at the higher temperature of $0.8\,T_c$. We see that the domain walls are becoming more ragged with random noise starting to decrease the coherence of domains. Despite this, coarsening does continue as before with the larger domains growing at the expense of the smaller ones much like in the simple model. The topological walls are again in evidence here, for example the −60° 1–2 walls at t=250 MCSPR.

As the temperature is further increased, thermal fluctuations increase until the domain structure breaks down and the ring spin configuration becomes disordered.

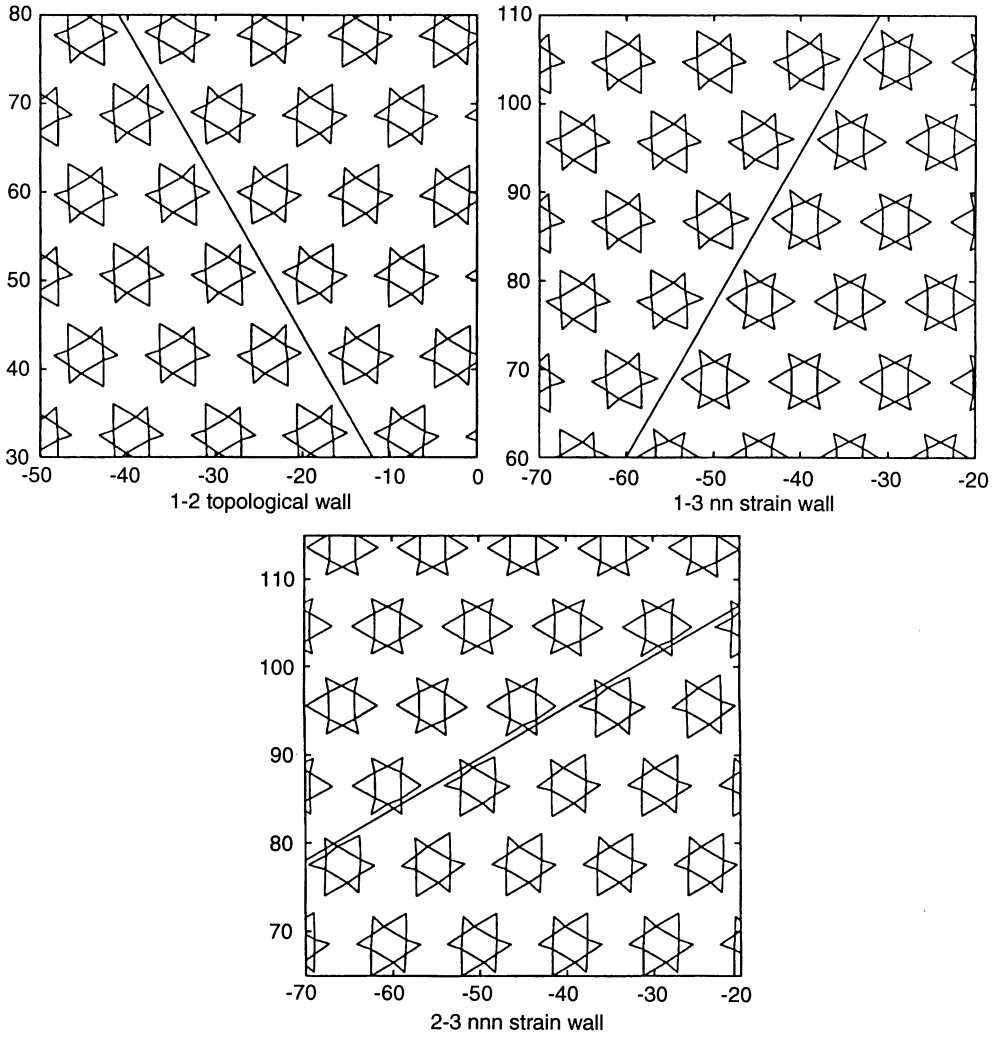

Fig. 15 The relaxed oxygen atom positions corresponding to the presence of a topological wall and the two types of strain wall. The *lines* show springs connecting oxygens in their triangles (other springs have been omitted for clarity). The *larger, swollen triangles* contain Al. The walls shown here correspond to the idealised case where they are perfectly thin and flat

6 Three dimensional structural model

6.1 Methodology

In the 3D structural model, we consider the entire cordierite structure as in Fig. 3. Again, the tetrahedra are considered to be very rigid and so the four oxygen atoms within them are connected via strong springs (k=100 rel. units). The T2 rings are also modelled as fairly rigid units with additional springs being placed around the outside and the inside of these rings much like in the 2D model.

As an additional piece of known physics we include extra springs between neighbouring tetrahedra placed so as to exclude nearest neighbour Al pairs by making such configurations have high energies. This exclusion is called *Loewenstein's rule* (1954) and has been observed experimentally in ordered cordierite as shown in Fig. 4. Apart from the common oxygen, the oxygen atoms are connected by springs from one tetrahedron to its neighbour in every combination. When two Al are next to each other, these springs stretch increasing the energy so the system tends to avoid these configurations thus preserving Loewenstein's rule.

The oxygens in the octahedra are also connected by springs though less rigidly than the tetrahedra (k=50 arb. units). Mg–O bonds are expressed as relatively weak springs (k=10 arb. units). Kanzaki forces are again applied so that when an Al is in the centre of a tetrahedron, the oxygen atoms are pushed outwards. No forces are applied by Si atoms. Again, we allow only Al pair rotations within the rings during Monte Carlo steps so that the two Al per ring always remain on opposite sides of their rings as shown in Fig. 5. The energy corrections are again calculated using Eq. 17.

Because the model is now three dimensional, we are free to choose any shape for the overall sample to be simulated. However since we are primarily interested in the domain formation within the T2 planes, a thin slab geometry is used parallel to these planes. The number of unit cells in the *c* direction is chosen so as to be large enough to avoid serious edge effects and allow interactions between layers to be expressed without making the simulation impossibly time consuming (this 3D model is very computationally intensive). A reasonable compromise between these factors turns out to be a hexagonal slab with 32 unit cells on a side in the a-b (T2) plane and 3 unit cells along the c direction. This gives 6 T2 ring layers interspersed with 7 T1-octahedra layers. The total number of atoms simulated is 408228.

6.2 Results and discussion

In each simulation presented, the domain patterns in all six T2 ring layers were almost exactly the same but with some deterioration of the domain structure in the layers near the surfaces. Therefore, the domain walls are always perpendicular to the T2 layers as expected. In the follow-

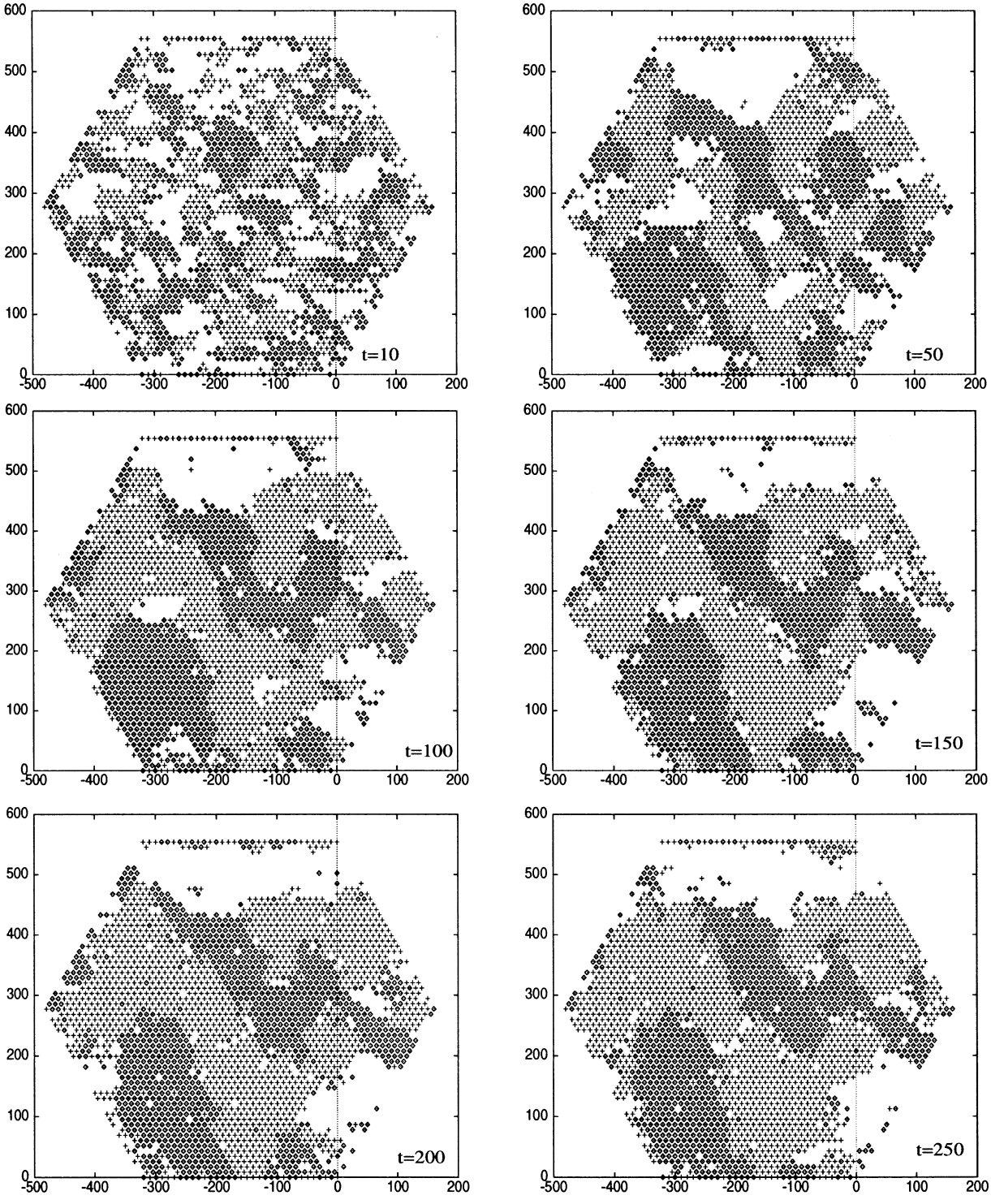

Fig. 16 Time evolution of the 2D structural model at around $T = 0.8\,T_c$, (°=type 1; +=type 2, blank=type 3)

ing figures, only the spins from the *central* T2 ring layer are shown.

Figure 17 shows the ring spin evolution for the 3D simulation below T_c. Domain formation and coarsening again proceed rapidly and again the domains consist of patches rather than the alternating stripes common in other structures. The domain walls are almost all topological walls. For example, looking at the t=60 MCSPR snapshot, we see a triangular type 1 domain at co-ordinate (0,300). The walls surrounding this domain are ±60° 1–2 walls and also 0° 1–3 walls all of which are along the Al–Al pair direction on one side of the wall. A little further down on the same picture, we observe 0° and +60° 2–3 topological walls.

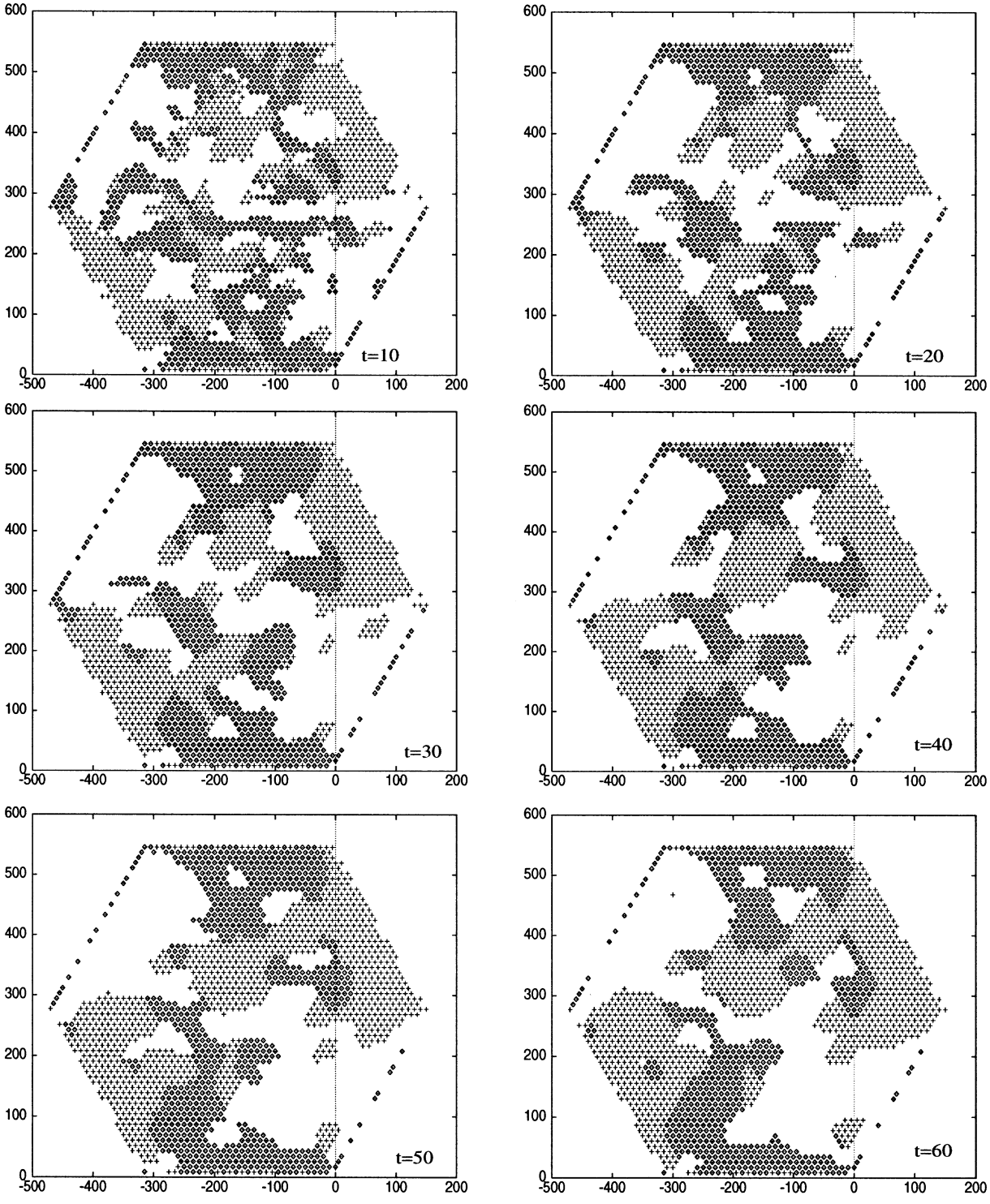

Fig. 17 The evolution of the central plane of T2 rings below T_c for the 3D model (°=type 1; +=type 2; blank=type 3)

Continuing the time evolution in Fig. 18, we see some more domain growth but there is another, rather curious type of motion. In the previous two simulations, the domains were very static: they simply formed and then grew in a particular part of the sample with larger domains growing at the expense of the smaller ones until only a few (usually three) domains survived. Here, however, the domains appear to be 'writhing' around: constantly changing their position and shape. For example, the large type 1 domain at the top right of the sample at t=110 MCSPR extrudes a large blob near the centre of the sample with then migrates towards the centre. The blob then unites with other type 1 domains at the bottom left of the sample giving rise to a very different

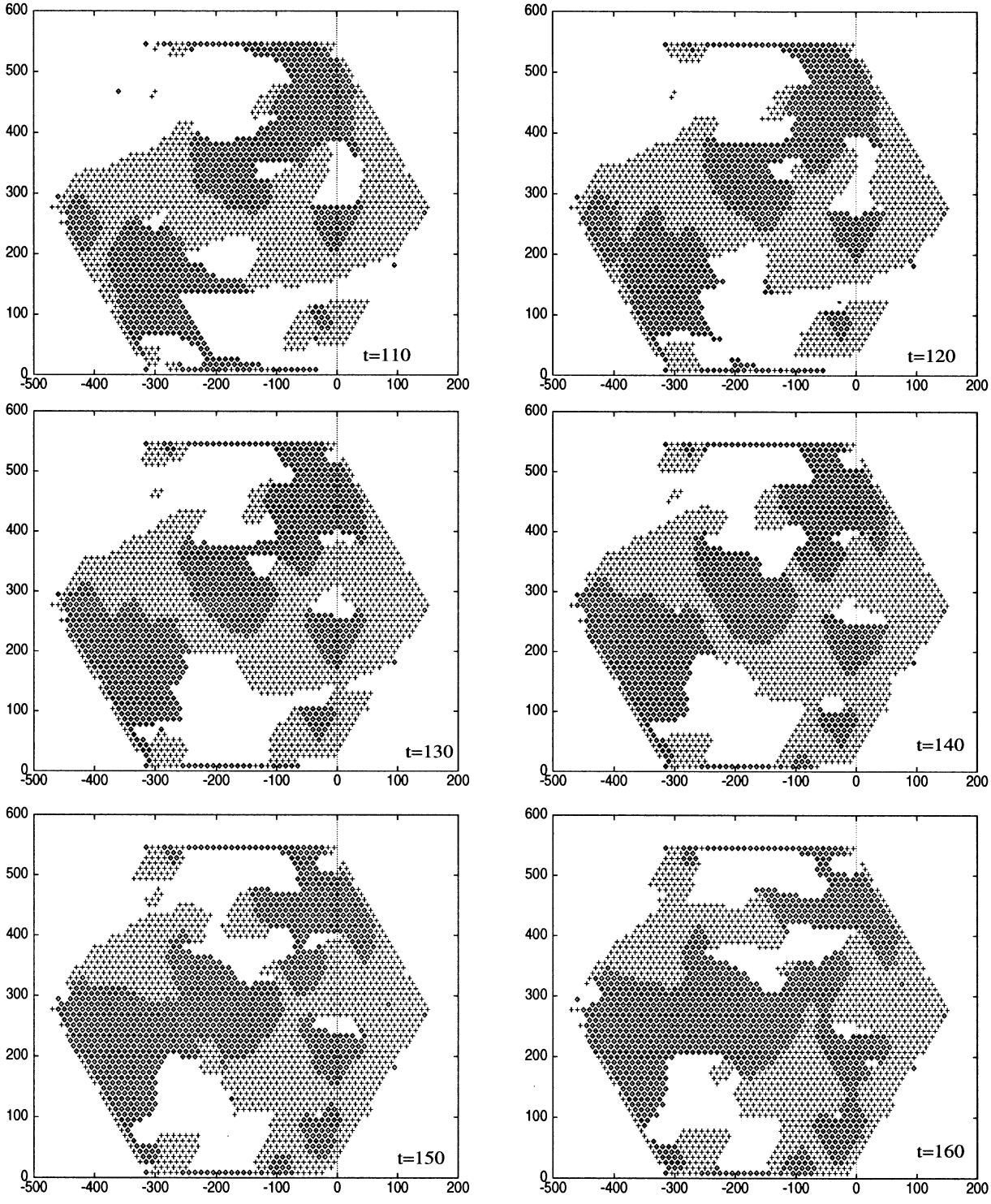

Fig. 18 Continuing the domain evolution from the previous diagram (°=type 1; +=type 2; blank=type 3)

type 1 distribution in t=160 MCSPR than in t=110 MCSPR. Similarly, the type 3 domain at top of the sample in t=110 MCSPR is rapidly superseded by the advancing type 2 domains coming upwards from the centre.

There is a very strong tendency for nearby domains of the same type to connect to each other and this is often done by forming finger-shaped extrusions which move towards each other and connect. The domains then rapidly flow together to form a single domain. For example, the type 3 domain at the top of the sample in t=110 MCSPR is bridged by t=160 MCSPR by two fingers of type 2 coming from the left and right. The leftmost of these two domains also links to the small type 2 patch emerging

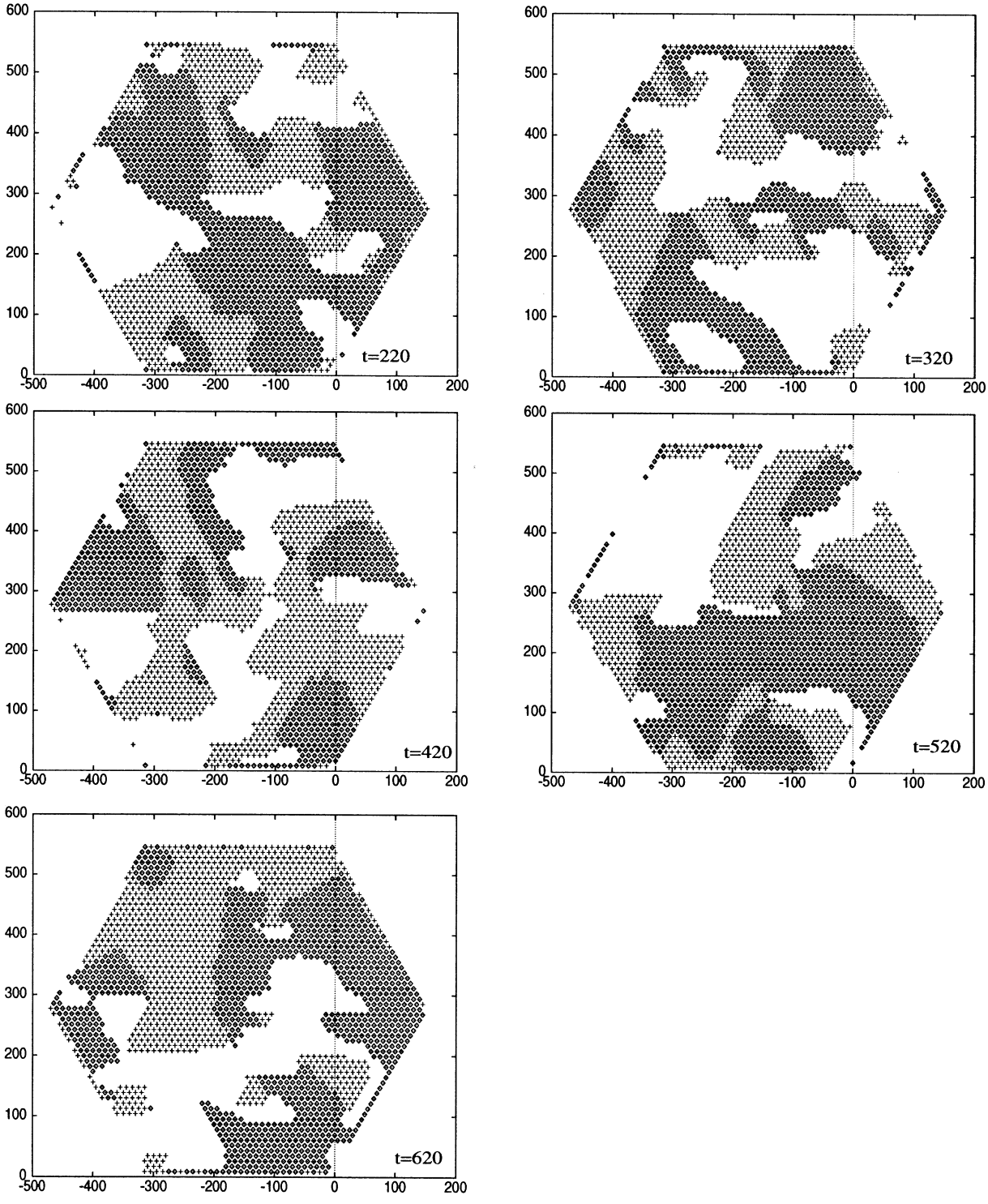

Fig. 19 Continuing the domain evolution from the previous diagram (°=type 1; +=type 2; blank=type 3)

at the top of the sample. The type 3 domain at (0,320) in t=110 MCSPR is also bridged by type two fingers splitting it into two domains.

This effect is very similar to the way in which two nearby drops of water tend to link and then flow into each other: i.e. the domains exhibit *surface tension* effects. This surface tension causes the domain walls to be much more rounded than in the previous two simulations making wall directions less clear. However we can continue to identify the topological walls and, to a limited extent, some nnn strain walls. For example, there is a +30° 2–3 nnn strain wall near the centre left of the t=110 sample.

Figure 19 shows the continued domain evolution for this simulation. The snapshot interval is 100 MCSPR

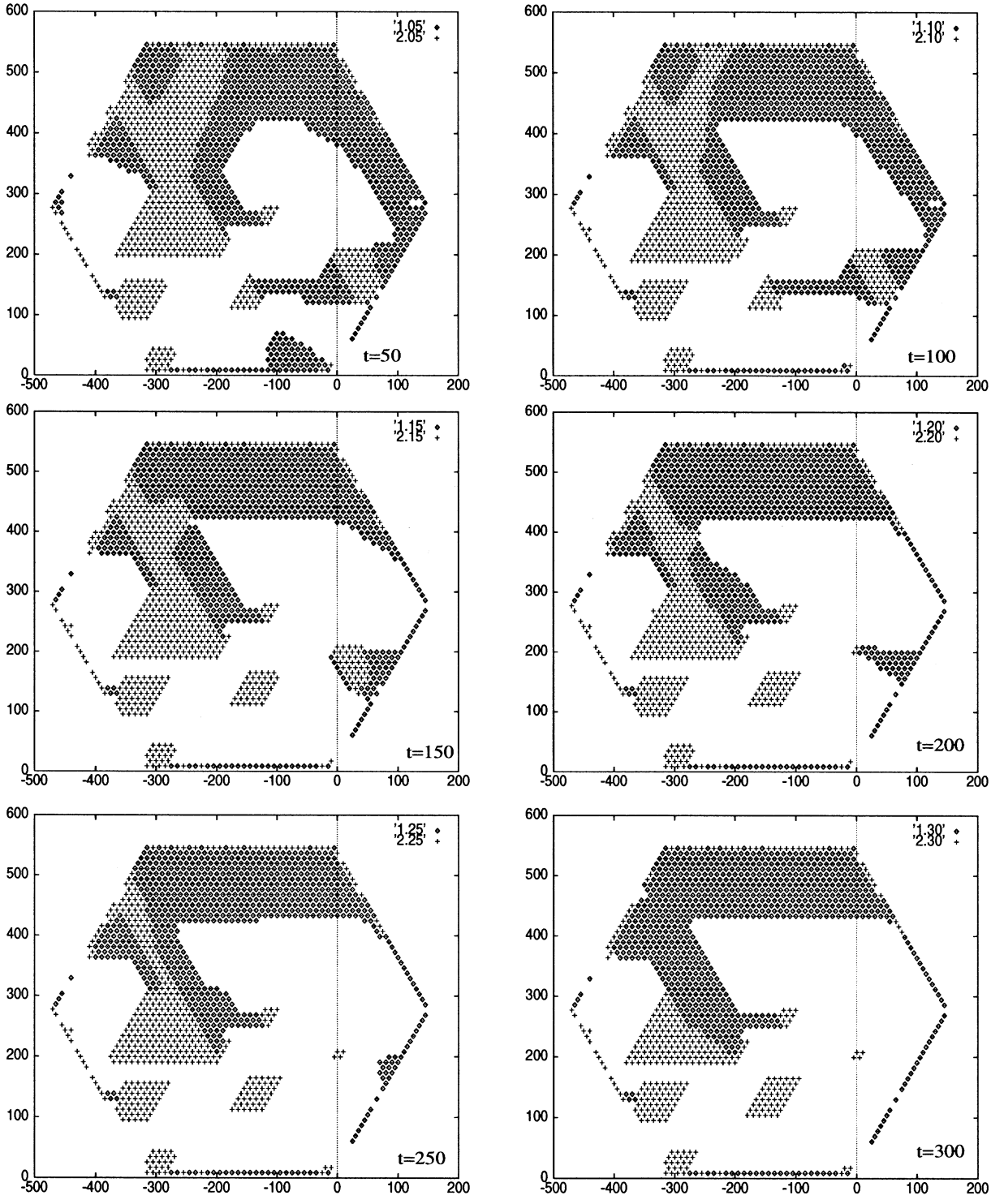

Fig. 20 Continuing the domain evolution from the previous diagram but at a much lower temperature (°=type 1; +=type 2; blank=type 3)

and the patterns in consecutive snapshots are totally different. As we go from one pattern to the other the three types of domain constantly advance upon each other just as described in Fig. 18 with no clear static domain positions or shapes being established.

We can again see the *nnn* strain and topological walls here but there is no sign of the *nn* strain walls which, as in the simplified, 2D model seem to be suppressed by the topological walls. For example, the ±30° nnn strain walls between 1–3 and 2–3 are present in the left of the *t*=220 MCSPR diagram and the +90° nnn strain wall is a little further up. Where *t*=320 MCSPR shows a network of −60° 1–2 topological walls and there is a large 0° 1–3 topological wall to the centre left of the *t*=420 MCSPR snapshot.

The fluctuations in these plots are, of course, driven by thermal effects. At lower temperatures, the domains do indeed settle down to form increasingly large fixed domains. Figure 20 which continues from Fig. 19 shows this. At this lower temperature, we see dominance of topological walls very clearly. For example there is a well-defined type 2 parallelogram at t=300 formed entirely of topological walls.

7 Discussion

We are now in a position to return to the experimentally observed domain structures shown in Figs. 1 and 2 and comment on their characteristics based on the results of the computer simulations.

Looking first at Fig. 2, which shows the strain modulation of twinned and tweeded cordierite, we recall our previous observation that the domain structure is very patchy with poorly defined wall directions. This observation is in striking contrast with the appearance of tweed in YBCO and feldspar (Putnis and Salje 1994) which show much more constrained modulations. This effect can now be explained in the light of our computer simulations. In the strain-mediated Potts model, there is only one atom per unit cell and so the only motion available to the simulation is strain which corresponds directly to the two acoustic modes of vibration that the structure possesses. This model therefore produces only strain-mediated walls in accordance with Sapriel's condition. However, the uncharacteristic patchiness is already apparent in this model simply because of cordierite's large number of strain walls (namely 6) compared to the two observed in structures with only two domain types. Because there are so many walls to choose from it is unlikely that the crystal will consist of areas with only one domain wall such as are observed in these two state structures. Therefore the patchy domain structure observed experimentally appears in even the simplest computer model studied.

As we proceed to increase the complexity of the structure simulated, additional mechanisms become apparent which further contribute to patchy rather than straight domain shapes. In the 2D structural model, the presence of cordierite's six-membered tetrahedral ring causes short range interactions to become important. Whereas strain interactions are independent of the detailed structure of the unit cell we observe additional, topological walls which are the result of 'rubbing' of neighbouring rings, a process which is highly dependent on the geometry of these ring structures. The presence of these characteristic ring structures results directly in doubling the number of possible domain walls from 6 to 12. This greater flexibility in possible wall direction makes patchy domain formation still more energetically favourable than in the simple model.

Finally, proceeding to the 3D structural model, we now allow layers of T2 rings to interact in the c-direction. The ordering process is always such that rings are stretched in the same way along the c-axis. Thus, *tubes* of T2 rings form into bulky, rigid structural units extending though the crystal. The direct rubbing together of these tubes represents an even greater fraction of the free energy total than in the 2D structural model and so the system is more likely to form topological walls which reduce the energy associated with these local interactions.

However, the formation of coherent T2 tubes in the 3D model introduces a new type of motion into the system which is not observed in the other structures simulated. The very strong local interactions between T2 tubes introduce a strong cohesiveness in the domains: the domains tend to hold together as well-defined areas even at comparatively high temperatures. Whereas in the other models, the thermal fluctuations at high temperatures appear as poorly defined domain walls and the appearance of random ring spins throughout the crystal, in the 3D model such fluctuations appear to cause entire domains to move around the sample and change their shapes while retaining very sharp domain walls. There are clear surface tension effects involved in this fluid-like motion which cause domains to become rounded and tend to move domain walls away from their expected soft directions.

In summary there appear to be two factors influencing patchy domain formation in cordierite: the large number of allowed domain walls, six strain walls and six topological walls and the 'writhing', fluid-like motion of domains caused by strong interactions between tubes of T2 rings observed in the 3D structure.

We now turn to the question of whether such ill-defined domain patterns also appear in natural cordierite samples on a macroscopic scale (e.g. as seen under an optical microscope). In particular we may ask if topological walls exist in geological samples. In the thin sections of Fig. 1, the dominant walls appear to be along the crystallographic {110} planes. The angle between {110} and planes connecting pairs of opposite Al in the rings averaged over subsequent layers along the c-axis is 60º (Gibbs 1966; Armbruster 1986). In Fig. 1a, the plane of the optical axes is 30º with respect to the twin walls between segments of the hexagon. In this configuration there are no domain walls which are parallel or perpendicular to the plane of the optical axes in adjacent domains (i.e. perpendicular or parallel to the Al—Al connecting vector). Hence all the walls in Fig. 1a are strain walls. In Fig. 1c, however, wall segments parallel to the Al–Al connecting vector *are* seen at some distance from the centre of the hexagon pointing vertically (marked as 1 and 2). Although the physical origin of these walls may be related to growth phenomena etc., their orientation is not compatible with the strain-free condition of ferroelastic twin walls. It is possible, therefore, that the formation of these walls is related to the appearance of topological walls in our computer simulation.

References

Armbruster T (1986) Role of Na in the structure of low cordierite: a single crystal X-ray study. Am Mineral 71:746

Binder K (1981) Static and dynamic critical phenomena of the two dimensional Q-state Potts model. J Stat Phys 24:69

Bratkovsky AM, Marais SC, Heine V, Salje EKH (1994a) The theory of fluctuations and texture embryos in structural phase transitions mediated by strain. Phys Condens Matter 6:3679

Bratkovsky AM, Salje EKH, Marais SC, Heine V (1994b) Theory and computer simulation of tweed texture. Phase Trans 48:1

Bratkovsky AM, Heine V, Salje EKH (1996) Strain effects particularly in phase transitions. Philas Trans R Soc London A 354: 2875

Daniels P, Maresch WV, Shreyer W, Sahl K (1992) Electron-optical and X-ray powder diffraction study of synthetic and natural potassium cordierite. Contrib Mineral Petrol 111:484

Eichhorn K, Binder K (1996) Monte Carlo investigation of the 3-dimensional random-field 3-states Potts model. J Phys Condens Matter 8:5209

Gibbs GV (1966) The polymorphism of cordierite I: the crystal structure of low cordierite. Am Mineral 51:1068

Müller WF, Schreyer W (1991) Microstructural variations in natural cordierite from the Eifel volcanic field Germany. Eur J Mineral 3:915

Nord GL (1994) Transformation-induced twin boundaries in minerals. Phase Transit 48:107

Parlinkski K, Heine V, Salje EKH (1993) Origin of tweed texture in the simulation of a cuprate superconductor. J Phys Condens Matter 5:497

Putnis A (1992) Introduction to mineral sciences. Cambridge University Press, Cambridge, UK

Putnis A, Holland, TJB (1986) Sector trilling in cordierite and equilibrium overstepping in metamorphism. Contrib Mineral Petrol 93:265

Putnis A, Salje E (1994) Tweed microstructure: experimental observations and some theoretical models. Phase Transit 48:85

Putnis A, Salje E, Redfern SAT, Fyfe CA, Stroble H (1987) Structural states of Mg cordierite I: Order parameter from the synchrotron X-ray and NMR data. Phys Chem Minerals 14:446

Redfern SAT, Salje E, Maresh W, Schreyer W (1989) X-ray powder diffraction and infrared study of the hexagonal to orthorhombic phase transition in K-bearing cordierite. Am Mineral 74:1293

Salje E (1987) Structural states of Mg cordierite II: Landau theory. Phys Chem Minerals 14:455

Salje E (1993) Phase transitions in ferroelastic and coelastic crystals. Cambridge University Press, Cambridge, UK

Salje E, Parlinski K (1991) Microstructures in high T_c superconductors. Superconductor Sci Techn 4:93

Salje EKH, Ishibashi Y (1996) Mesoscopic structures in ferroelastic crystals: needles twins and right-angle domains. J Phys Condens Matter 8:1

Salje EKH, Buckley A, van Tendeloo G, Ishibashi Y, Nord G (1998) Needle twins and right-angled domains in minerals: comparison between experiment and theory. Am Mineral submitted

Sapriel J (1975) Domain-wall orientations in ferroelastics. Phys Rev B 12:5128

Schreyer W (1986) The mineral cordierite – structure and reactions in the presence of fluid phases. Ber Bunsenges 90:748

Thayaparam S, Heine V, Dove MT, Hammonds KD (1996) A computational study of Al/Si ordering in cordierite. Phys Chem Minerals 23:127

Tsatskis I, Salje E (1996) Time evolution of twin domains in alkali feldspars: a computer simulation study. Am Mineral 81:800

Tsatskis I, Vul DA, Salje EKH, Heine V (1994) Geometrical coupling between inhomogeneous strain fields: application to fluctuations in ferroelastics. Phase Transit 52:95

Venkatesh V (1954) Twinning in cordierite. Am Mineral 39:636

Vul DA, Salje EKH (1995) Periodic twin microstructures in YBCO thin films: a computer simulation study. Physica C 253:231